AIAA JOURNAL
Vol. 44, No. 11, November 2006

Experimental Study of Underexpanded Supersonic Jet Impingement on an Inclined Flat Plate

Yusuke Nakai,* Nobuyuki Fujimatsu,† and Kozo Fujii‡
Institute of Space and Astronautical Science, Japan Aerospace Exploration Agency, Kanagawa 229-8510, Japan

DOI: 10.2514/1.17514

Flowfields of the M2.2 jet impinging on an inclined flat plate at various plate angles, nozzle-plate distances, and pressure ratios are experimentally investigated using pressure-sensitive paints and Schlieren flow visualization. The effect of temperature variation on the flat plate is eliminated by the calibration using temperature-sensitive paints. A comparison with the former experiment shows that the current pressure-sensitive paint measurement produces reliable data sufficient for the flowfield discussion under consideration. The pressure-sensitive paints and Schlieren images obtained in the experiment suggest that the flowfields at various flat plate angles, nozzle-plate distances, and pressure ratios can all be classified into three types of flow structure. Within the range of geometrical and flow conditions considered in the present paper, the flowfield patterns can be predicted without experiments if the shock cell length in the freejet for various pressure ratios is known in advance. Extensive studies for a wide range of geometrical and physical parameters became feasible with a new efficient pressure/temperature-sensitive paint measurement technique showing surface pressure map with much less effort compared to conventional pressure tap measurement.

Nomenclature

D_n	=	nozzle exit diameter
I	=	luminescence intensity
I_{ref}	=	reference luminescence intensity
L	=	nozzle-plate distance
L_s	=	shock cell length of the freejet
L'_S	=	distance from the nozzle exit to the location of maximum diameter of first barrel shock
P	=	pressure
P_c	=	total pressure
P_{ref}	=	reference pressure
R_n	=	nozzle exit radius
T	=	temperature
T_{ref}	=	reference temperature
x	=	vertical distances from the jet exit to the location of the jet hitting the plate
y	=	length along the wall
θ	=	inclined angle of plate

I. Introduction

FLOWFIELDS created by supersonic jets impinging on an inclined flat plate appear in various industrial applications. Examples can be found in plume-wall interactions during multistage rocket separation at high attitude and space module attitude-control thruster operation, among others. Generally, these flowfields are extremely complex due to the existence of mixed subsonic and supersonic regions, interacting shock and expansion waves, and strong shear layers. Although there are many papers published in this research field [1–4], most of them used array of pressure taps for surface pressure measurement over the plate and their discussions were based on limited pointwise information under limited flow conditions. Recently, there appeared studies using numerical simulations [5,6]. They are, however, intended to reproduce the results presented in the former study by Lamont and Hunt [3] and only limited cases were considered probably due to large computer time required for the numerical simulations. Jet impingement essentially depends on three parameters: pressure ratio, nozzle-plate distance, and flat plate angle. Experimental reports, particularly on supersonic jet impingement at high-pressure ratios are not available and details of the flow structure at various parameters have not been discussed.

Recently, new techniques of surface pressure or temperature measurement called pressure/temperature-sensitive paint [PSP/TSP] techniques have been developed and discussed [7]. PSP/TSP techniques are based on oxygen/thermal quenching of photoluminescence. This technique can easily supply us with surface pressure distributions as an image with high spatial resolution, compared with the use of conventional pointwise measurement systems such as pressure taps.

In the present study, PSP/TSP techniques are applied to measurement of surface pressure and temperature over an inclined flat plate located underneath a supersonic impinging jet. Experiments are conducted for a much wider range of pressure ratios, nozzle-plate distances, and plate angles compared to the studies in the past. Measurement data obtained by the PSP method are strongly influenced by temperature variation on a model surface [8]. Thermocouple measurement was tried to remove the temperature dependency of PSP measurement [9], but the results were not satisfactory due to the lack of accuracy and spatial resolution. Here, TSP measurement is used for temperature calibration to improve the quantitative reliability of PSP measurement.

In addition to the PSP/TSP measurement, Schlieren images are taken to identify the flow structure inside the jet. The flow configuration in this study is similar to what was used by Lamont and Hunt [3]; however, the flowfields under relatively higher pressure ratios are discussed in detail and classified into several flow patterns for three important parameters: pressure ratio, inclined angle, and distance of the flat plate to the jet.

Presented as Paper 3467 at the Aerospace Sciences Meeting 03, Reno, NV, 6–10 January 2003; received 4 May 2005; revision received 3 May 2006; accepted for publication 3 August 2006.

*Former Research Student at the ISAS, Graduate Student, Department of Mechanical Engineering, Tokyo University of Science; currently Honda R&D Company, Ltd. Student member AIAA.

†Research Associate; currently Research Associate at Aoyama Gakuin University. Member AIAA.

‡Professor. Fellow AIAA.

II. PSP/TSP Measurement System

A. Principle of PSP/TSP

The PSP/TSP measurement mechanism is based on the oxygen and thermal quenching of luminescent molecules [10]. Existing typical PSP sensors consist of two main elements, an oxygen sensitive fluorescence molecules (molecular sensor = paint) and an oxygen permeable binder (binder). When a light source of appropriate energy wavelength excites these luminescent molecules, luminescence emission occurs. Luminescence intensity is inversely proportional to the partial pressure of oxygen in air [8].

The relationship between luminescence intensity and oxygen partial pressure is described in a form with a nonlinear effect considered as follows.

$$\frac{I_{P,\mathrm{ref}}}{I_P} = \sum_{k=0}^{n} A_k(T)\left(\frac{P}{P_{\mathrm{ref}}}\right)^k \tag{1}$$

The TSP relation between luminescence intensity and temperature is also described similarly to Eq. (1).

$$\frac{I_{T,\mathrm{ref}}}{I_T} = \sum_{k=0}^{n} B_k\left(\frac{T}{T_{\mathrm{ref}}}\right)^k \tag{2}$$

A_k in Eq. (1) and B_k in Eq. (2) are determined by either a priori measurement using a static calibration test carried out in advance or in situ measurement using pressure tap data simultaneously obtained during the experiment. In this study, an a priori method is adopted and quadratic polynomial ($n = 2$) curves are used for calibration. Bathophen Ruthenium Chloride [Ru(dpp)] and a thin layer chromatography plate (TLC plate) are used as the PSP luminophore and binder, respectively.

Two types of TSP: Europium Thenoyltrifloroacetonate (EuTTA)/Dope and EuTTA/PMMA, are tested for the temperature measurement over a flat plate surface. The temperature measurement is carried out mainly to eliminate the temperature influence on the pressure measurement.

B. Experimental Setup

Experiments are carried out using a small induction-type wind tunnel shown in Fig. 1. A schematic of a close-up view of the experimental setup is shown in Fig. 2. The test section is connected to a large low-pressure chamber and dried air (therefore ratio of specific heats is 1.4) is supplied into the test section. The total pressure of the nozzle flow is kept constant and the ambient pressure near the flat plate is varied for suitable setup of the pressure ratio of the nozzle exit and ambient pressure. The conical nozzle with a design Mach number of 2.2 shown in Fig. 3 is connected to the settling chamber where the pressure is kept at 100 KPa. The throat diameter is 5 mm and the nozzle exit diameter is 7.08 mm. A flat plate of 200 mm squire is placed on an electrically controlled stage in the test section. TLC plate of 100 mm squire is glued over the plate. The location and angle of the flat plate are changed in the ranges of L/D_n from 1.0 to 4.5 and θ from 30 to 60 deg ($\theta = 90$ deg corresponds to the case of the flat plate being perpendicular to the jet flow) using a PC. A CCD camera for capturing the luminescence of the PSP/TSP is placed on top of the test section and images of roughly 100 mm by 100 mm squire are taken.

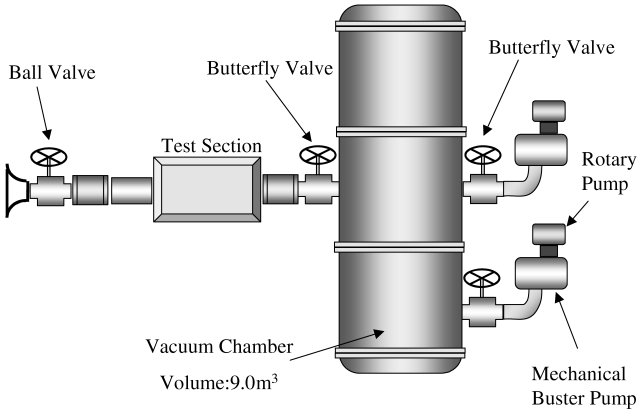

Fig. 1 Schematics of the induction-type wind tunnel.

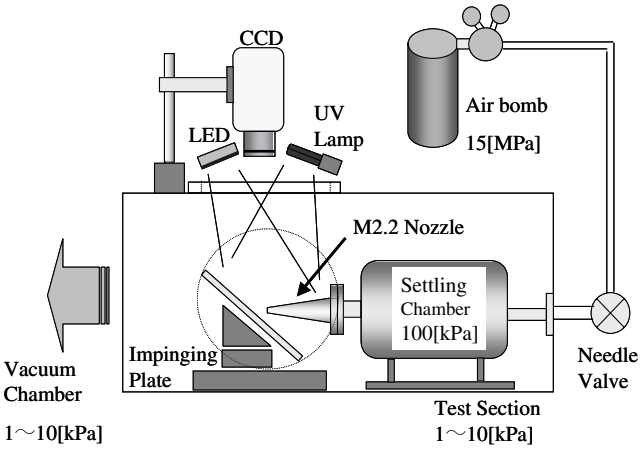

Fig. 2 Schematics of the test section and measurement systems.

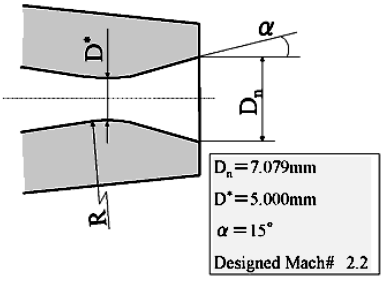

Fig. 3 Supersonic nozzle configuration.

Schematic of the static calibration system for obtaining the parameters A_k and B_k that determine the static characteristic curves of the PSP/TSP is shown in Fig. 4. Paint samples are placed in a pressure chamber where both pressure and temperature are controlled by a vacuum pump and a heat pipe. This calibration system consists of a vacuum chamber separated by two windows, which prevents moisture in the air from crystallizing on the window surface. Calibration is carried out in the pressure range from 1 to 100 KPa and in the temperature range from 283 to 298 K.

In both the calibration and the main experiments, the same optical system is used. Blue LED arrays and a UV lamp are used as excitation light sources for the PSP and TSP, respectively. A CCD digital camera detects emissions from the sample. The camera has 1024×1024 pixels resolution and 12-bit intensity resolution. A 650 ± 20 nm band-pass filter is placed in front of the camera object lens and the paint emission is separated from excitation light. Exposure time for the CCD camera is about 100 ms. PSP and TSP sensors are painted half by half over the flat plate and PSP and TSP measurements are carried out simultaneously.

All the images taken by the CCD camera are postprocessed with the software "SMAP," newly developed to improve conventional noise filtering method [11].

In addition to the pressure measurement over the plate surface, flow visualization with the Schlieren system is carried out and images of the cross section of the flowfields are obtained. Schlieren images are not taken simultaneously with the PSP/TSP measurement but taken consecutively. PSP images have only 12 bits spatial resolution and might lose details of flow changes like shock reflections over the plate surface. Schlieren images combined with

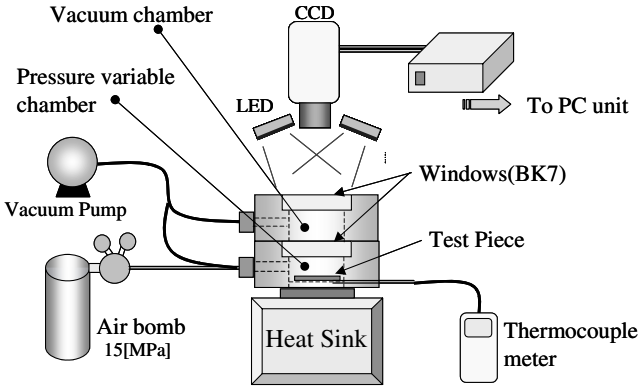

Fig. 4 Schematics of the calibration system.

the PSP measurement remove uncertainty of PSP measurement and help understanding of flow structures.

III. Result and Discussions

A. PSP/TSP Calibration

Figures 5 and 6, respectively, show the temperature and pressure sensitivities of the combinations of the PSP/TSP molecular sensors and binders. The reference pressure is 100 KPa, and the reference temperature is 298 K. Although the combination of bathophen ruthenium chloride and the TLC plate has high pressure sensitivity (Fig. 5), luminescence intensity is strongly influenced by temperature variation as shown in Fig. 6. To remove the temperature dependency of the PSP, both EuTTA/Dope and EuTTA/PMMA combinations were employed as TSP sensors. Figure 6 shows that both the TSP combinations have appropriate temperature sensitivities. EuTTA/Dope is not used in the present experiment as it has a strong pressure dependency as shown in Fig. 5. The pressure dependency of the EuTTA/PMMA is sufficiently small for the pressure range used in the present experiment and therefore chosen for the present experiment.

B. Accuracy of PSP

Figure 7 shows an example of the measured pressure and the temperature maps on the inclined plate surface at a pressure ratio of 1.2. This pressure ratio is relatively low compared with those discussed in following sections, but was chosen because there were reliable experimental data available [3]. The left half of Fig. 7 shows

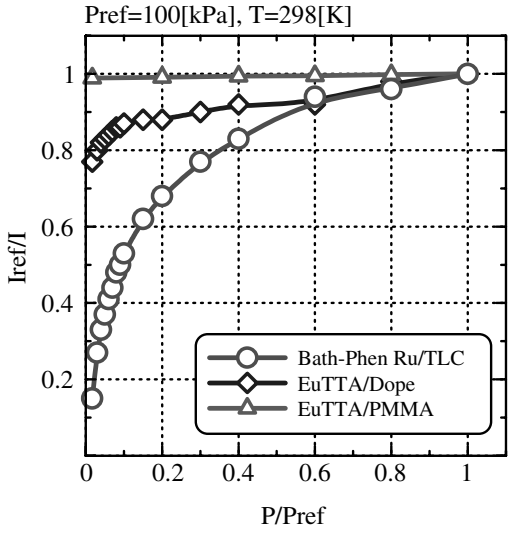

Fig. 5 Pressure sensitivity.

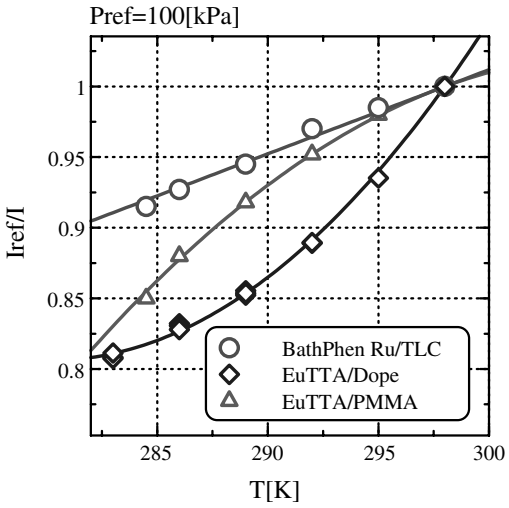

Fig. 6 Temperature sensitivity.

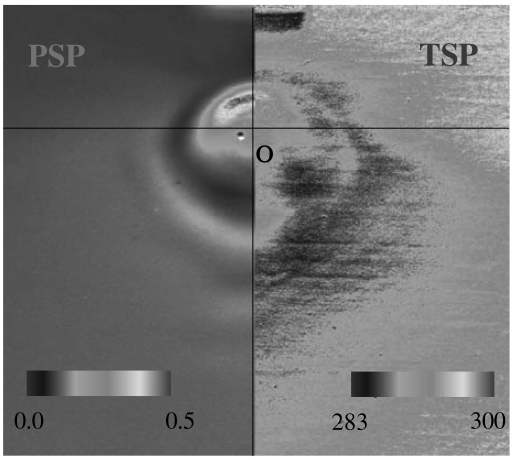

Fig. 7 Pressure and temperature maps on the plate surface ($\theta = 45$ deg, $L/D = 2.0$, PR $= 1.2$).

the pressure map obtained by the PSP technique and the right half of Fig. 7 shows the temperature map obtained by the TSP technique. The origin "O" shows the point where the extension of the nozzle centerline crosses the plate surface. The nozzle can hardly be seen in the top region of Fig. 7. Pressure peak and expansion regions as well as recompression shock waves can be successfully captured by the PSP measurement.

From the temperature map, the maximum temperature variation on the plate surface is about 10 K. As the luminescence intensity changes from 0.5 to 1.0% per Kelvin for the combination of the ruthenium sensor and TLC plate (as shown in Fig. 6), the effect of temperature variation on the plate surface is not negligible and may cause an error in the PSP measurement, which indicates that temperature calibration is necessary for quantitative discussions.

Figure 8 shows a comparison of the pressure distributions along the model centerline obtained by the present PSP measurement and the former experiment. The dashed line shows the result obtained using the pressure taps by Lamont and Hunt [3]. The dotted line shows the original data without temperature calibration and the solid line shows the data modified using the calibration curve obtained by the a priori experiment using the static cell shown in Fig. 4. Pressure is normalized by the pressure in the settling chamber (P_c). The horizontal axis y/R_n denotes the normalized distance along the model centerline measured from the origin. Although the result without the temperature calibration captures the qualitative feature of the pressure distribution, the discrepancy between the noncalibrated pressure distribution and that obtained using pressure taps is

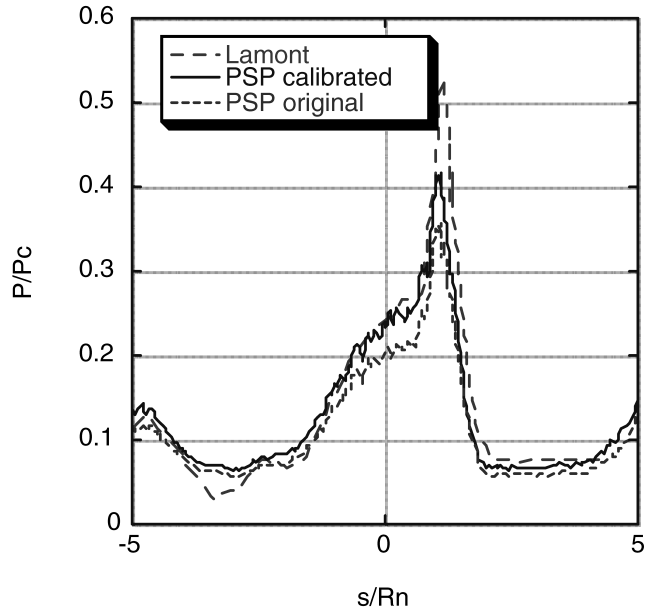

Fig. 8 Pressure distributions along the model centerline.

remarkable, particularly near the stagnation region. The calibrated result shows that the discrepancy is reduced when the temperature calibration is performed and it agrees well with Lamont's experimental data obtained using pressure taps, except near the pressure peak. The discrepancy of the peak pressure is roughly 20% and shows the difficulty in capturing a spikelike peak by the PSP measurement using pixel images. Note that the pressure distribution shown in Lamont's experiment in [3] is plotted as an interpolated curve based on the measurement using a limited number of pressure taps. Because only five pressure taps were used in a single unit of y/R_n of Fig. 4 in the Lamont experiment, pressure peak presented in his plot might be fictitious. There are 35 pixels in a single unit of y/R_n in the present experiment. Both the noncalibrated and calibrated results show the quantitative difference in the region $y/R_n = -3.0$ where a weak shock reflection exists although both capture the features of shock reflections. The result shows that the data obtained by the PSP measurement (with the temperature calibration) essentially capture the basic features of the flowfield and can be used for discussing flow structures.

It should be noted that all the plots in the following sections are based on the TSP calibrated data.

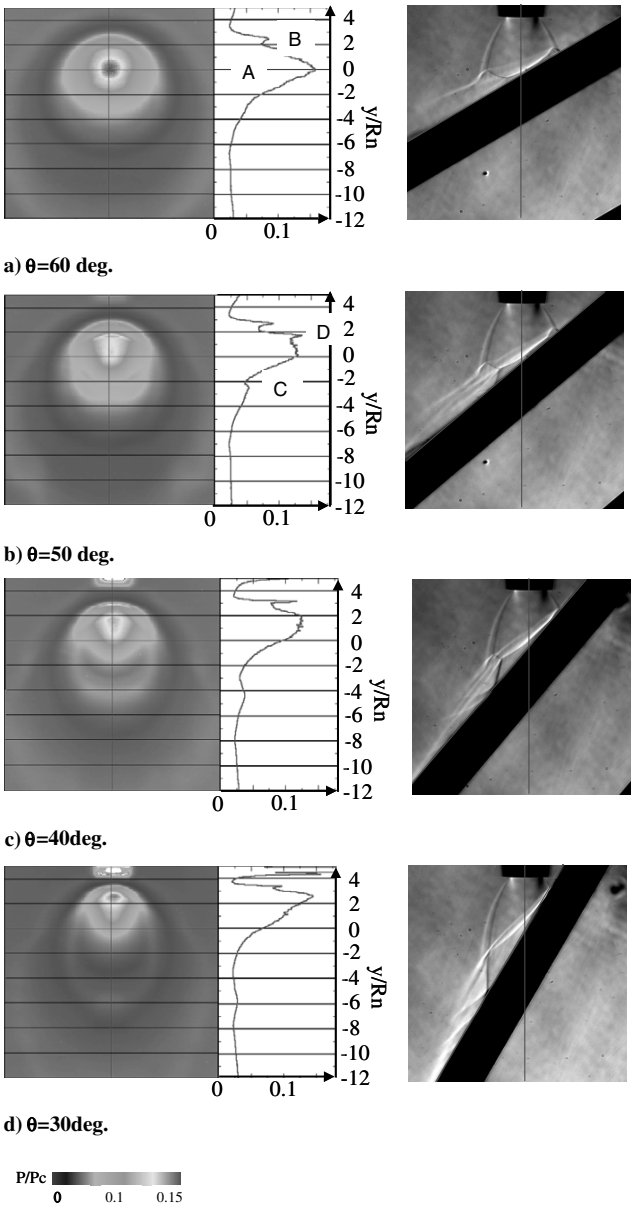

Fig. 9 Pressure maps and Schlieren images under various plate angles ($L/D = 2.0$, PR = 7.0).

IV. Flowfields

A. Effect of Plate Angle

The results of the experiment at various plate angles are discussed in the present section. The experiments are carried out at a fixed nozzle-plate distance of $L/D_n = 2.0$ and a nozzle exit to ambient pressure ratio (PR) of 7.0. Flat plate angle is changed from 30 to 60 deg at 5-deg intervals.

The surface pressure maps and the pressure distributions along the centerline (y/R_n-axis) obtained by the PSP measurement are shown in Fig. 9 at the cases of four different plate angles. The corresponding Schlieren images across the test section are also attached on the right-hand side of Fig. 9. On the basis of the obtained images shown in Fig. 9, schematics of the flowfields are produced and shown in Fig. 10. Generally, an underexpanded supersonic freejet forms shock cell structures with barrel shocks (or jet shocks) and Mach disks. A flat plate is located in the first shock cell structure of the freejet in all the cases considered here.

At $\theta = 60$ deg, the impinging jet generates shock waves over the flat plate. The main shock wave is called the plate shock and the others are called the upper or lower tail shock waves. This flowfield is called Type I in the present paper as is shown Fig. 10. The Type I flowfield has two pressure peaks on the flat plate. The pointwise pressure peak A is the highest pressure peak on the flat plate and is considered to be generated by the stagnation of the flow impinging on the plate, from the PSP images and the pressure distribution along the centerline shown in Fig. 9a. The other pressure peak B at $y/R_n = 2.5$ in Fig. 9a is created by the arc-shaped stagnation near the jet boundary on the plate. The Type I flowfield is frequently observed when the plate is nearly perpendicular to the jet, the nozzle-plate distance is large, and the pressure ratio is low.

As plate angle decreases, the flowfield becomes a Type II (with bubble) flowfield. At $\theta = 50$ deg, the wall jet expands along the plate surface and generates an intermediate tail shock wave emanating from the triple point generated at the end of the plate shock wave. Flows below the plate shock wave are supersonic at this flow condition. Reflections of the intermediate tail shock wave appear between the slip line and the wall. Shock wave reflections generate a sequence of pressure peaks with the strongest one being observed as another pressure peak C at $y/R_n = -2.5$ in Fig. 9b. As can be seen in the Schlieren image in Fig. 9b, a convex plate shock region is formed where the plate shock and barrel shock interact in the upstream region. This convex plate shock region is considered to have appeared because of the existence of a recirculation flow region called the "stagnation bubble" region. In the previous studies, it was

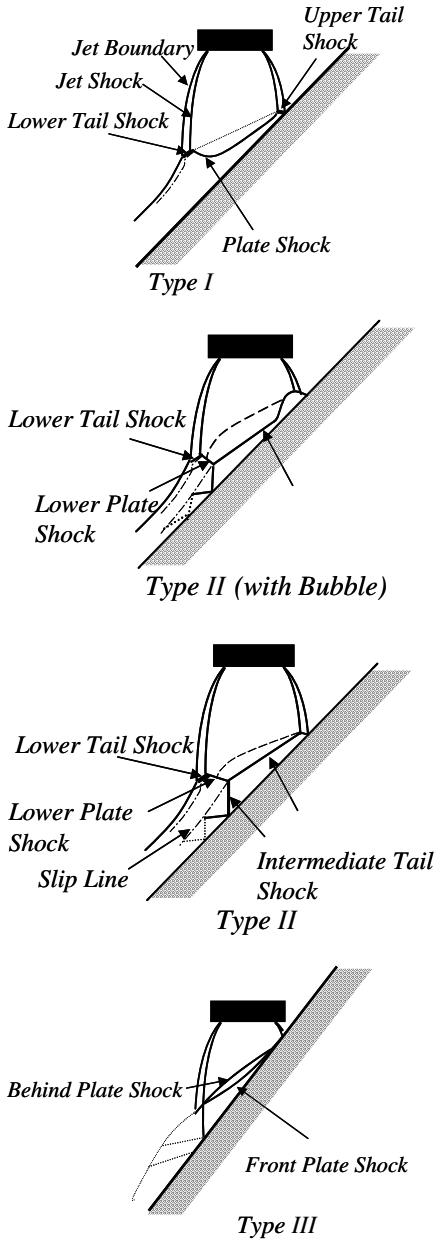

Fig. 10 Schematic picture of the typical flow structure.

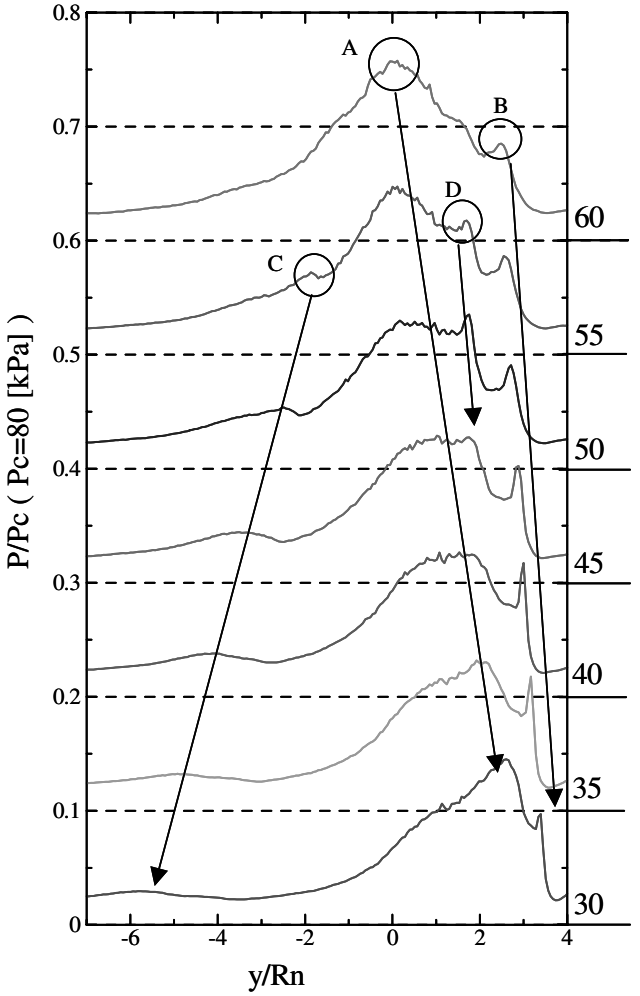

Fig. 11 Pressure distributions in the y/R_n axis for plate angle variations (vertical axis is 0.1 shifted up for each curve).

reported that stagnation bubbles are often observed at a high-pressure ratio condition when the flat plate is located nearly perpendicular to the jet. Tsuboi et al. reported that the existence of these bubbles strongly influences the surface pressure on the plate [12]. Existence of stagnation bubbles like those at a high pressure ratio and a plate angle such as in the present case has not yet been reported. Another pressure peak D is observed at $y/R_n = 1.5$ and becomes almost the highest of all the pressure peaks under this condition where the stagnation bubble appears. Although not presented in this paper, our CFD simulation conducted later confirmed that a recirculating flow occurs in this convex plate shock region.

At $\theta = 40$ deg, the pressure peak D formed by a stagnation bubble in the upstream region is not clearly observed, although the whole shock wave structure remains. The flowfield is also classified as Type II in Fig. 10.

At $\theta = 30$ deg, the intermediate tail shock wave merges with the barrel shock wave as the crossing angle of these shock waves decreases. The flowfield is of the Type III, as shown in Fig. 10. Under this flow condition the pressure peak A at $y/R_n = 2.5$ again becomes the highest peak.

To specify the location of pressure peaks at various angles, the pressure distributions along the y/R_n axis at 5-deg intervals from 30 to 60 deg are summarized in Fig. 11. Each curve is plotted at $P/P_c = 0.1$ intervals. The changes in location and strength of the pressure peaks with increasing the plate angle are clearly observed. The pressure peak D is only observed when a stagnation bubble appears under the condition of $\theta = 40$–50 deg.

B. Effect of Pressure Ratio

From the preceding discussions, it is clear that the flowfield generated by the supersonic jet impinging on the inclined flat plate at various plate angles can be classified roughly into three types. Each type can be distinguished by the shock wave configuration and the pressure distribution over the flat plate. In fact, the experiment carried out under other conditions with different nozzle-plate distances and/or pressure ratios showed that the observed flow patterns are limited to the three types. Flowfields at various pressure ratios are discussed hereafter. Experiments are carried out under the conditions of a fixed plate angle of $\theta = 45$ deg, nozzle-plate distance, a fixed nozzle distance of $L/D_n = 2.0$, and various pressure ratios from PR = 1.0 to PR = 10.0 at 1.0 unit intervals. Figure 12 shows the Schlieren images and pressure maps obtained by the PSP measurement. At PR = 1.2, a flowfield similar to the Type I flowfield (schematically shown in Fig. 10) is observed. Although this flowfield has a shock wave structure similar to Type I, the surface pressure distribution is different from that of Type I shown in Fig. 9.

As pressure ratio increases, the resultant flowfield becomes a Type II flowfield. The pressure map in this case has typical Type II

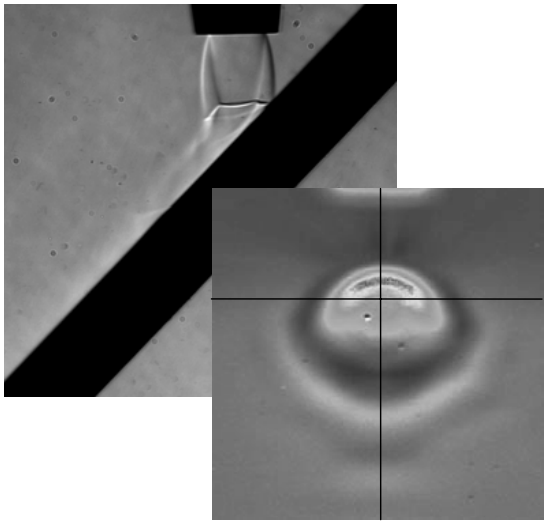

a) PR=1.2

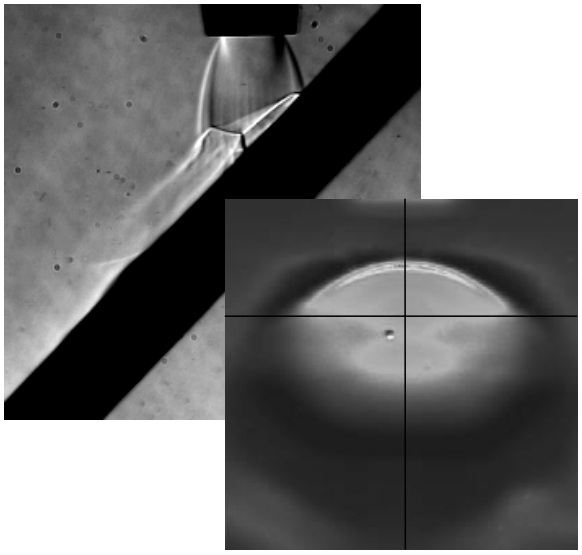

b) PR=4.0

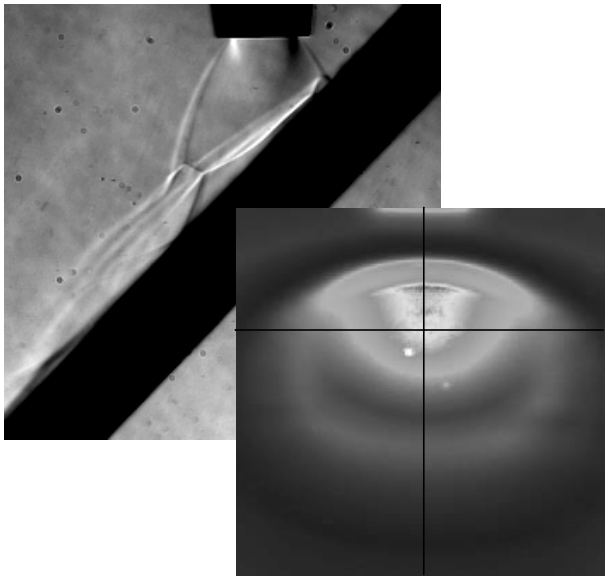

c) PR=10.0

Fig. 12 Flowfields at various pressure ratios ($L/D = 2.0$, $\theta = 45$ deg).

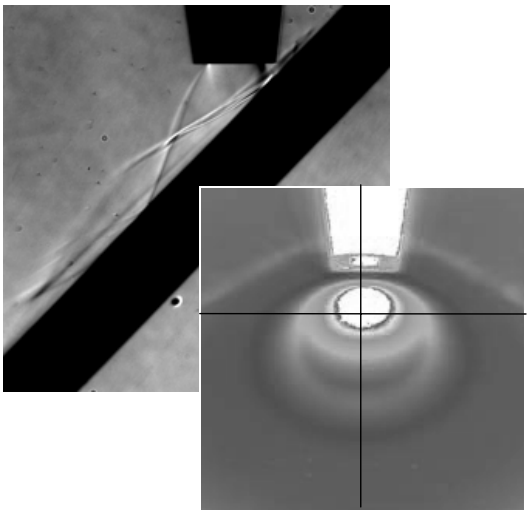

a) L/D=1.0

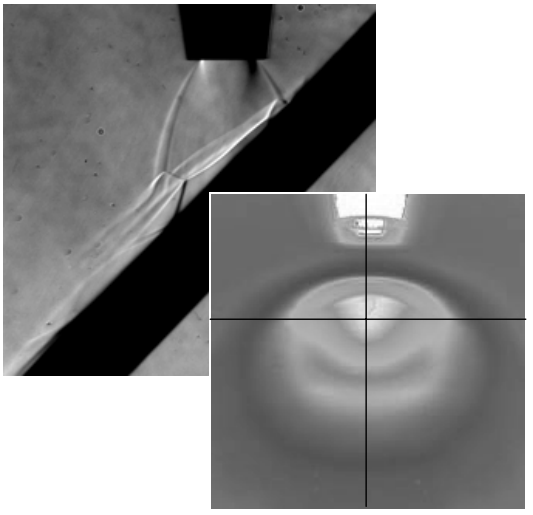

(b) L/D=2.0

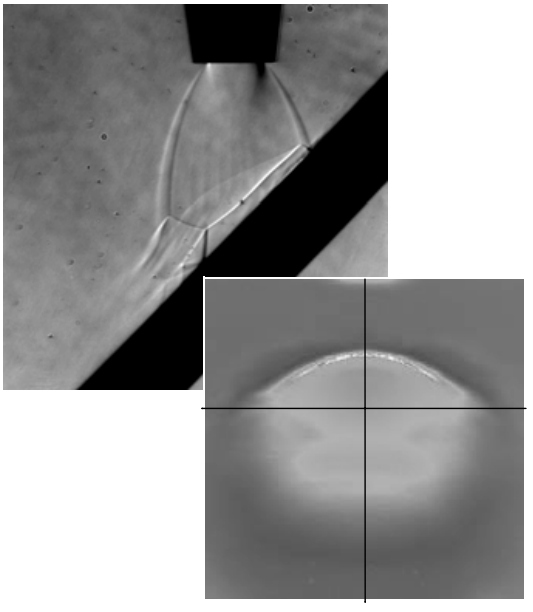

(c) L/D=3.0

Fig. 13 Flowfields at various nozzle-plate distances (PR = 8.4, $\theta = 45$ deg).

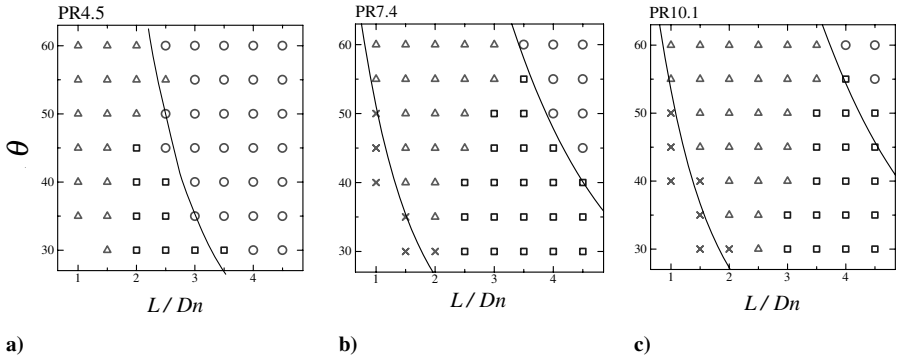

Fig. 14 Classifications of the flow patterns for three pressure ratios (circles: Type I, squares: Type II, triangles: Type II with bubble, crosses: Type III).

pressure distributions similar to the flowfield at $\theta = 50$ deg shown in Fig. 9b. The Type II (with bubble) flowfield can still be seen at PR = 10.0. Although the Type III flowfield did not appear in this experiment, it can frequently be observed when L/D_n is much lower. Generally, as pressure ratio increases, the flowfield gradually changes from Type I to Type III.

C. Effect of Nozzle-Plate Distance

To investigate the effect of nozzle-plate distance, experiments are carried out under a fixed pressure ratio of PR = 8.4, a fixed plate angle of $\theta = 45$ deg, and various nozzle-plate distances at 0.5 intervals. Three types of flow structure are observed in the Schlieren pictures and PSP images. Figure 13 shows that the flowfield changes from Type III to Type II (with bubble), then to Type II as the nozzle-plate distance increases. Type I appears at a larger distance than $L/D_n = 3.0$ although not shown here. The pressure distributions of each case are similar to those of each type for the flowfield discussed in preceding sections.

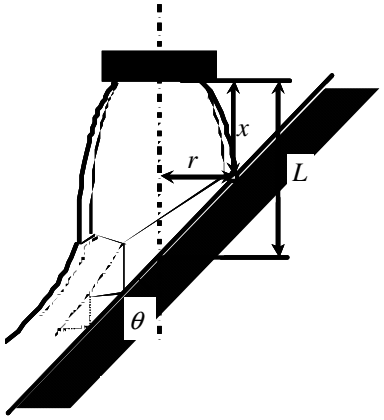

Fig. 15 Dominant parameters defining the flow patterns.

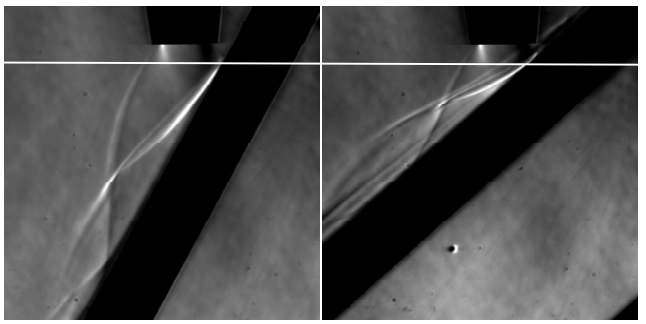

a) θ = 30 deg, L/d=2.0 b) θ=50 deg, L/d=1.0

Fig. 16 Type III flowfields at different conditions (PR = 7.0).

D. Correlation of the Parameters

On the basis of the observation of the Schlieren images with the aid of the pressure distributions over the plate obtained by the PSP measurement, the symbols of each flow type are plotted for various flat plate angles and nozzle-plate distances under given pressure ratios. Figures 14a–14c show results for the flow types at PR = 4.5, PR = 7.4, and PR = 10.1, respectively. The horizontal axis is the nozzle distance L/D_n, and the vertical axis is the plate angle θ. Solid lines are the curves of x/D_n being constant. x is the vertical distance from the nozzle lip to the point that jet boundary first impinges on the plate as shown in Fig. 15. Purpose of these plots will be presented later. The Type I flowfield mainly appears when the pressure ratio is low. As pressure ratio increases, Type II and Type III flowfields appear and becomes dominant under the conditions considered in the present paper.

Figures 16a and 16b show Schlieren images showing the same Type III flowfields, but under different conditions. PR is 7.0 for both

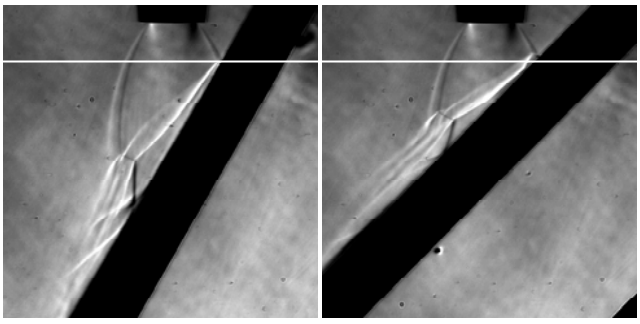

a) θ= 30 deg, L/d=3.0 b) θ=45 deg, L/d=2.0

Fig. 17 Type II flowfields at different conditions (PR = 7.0).

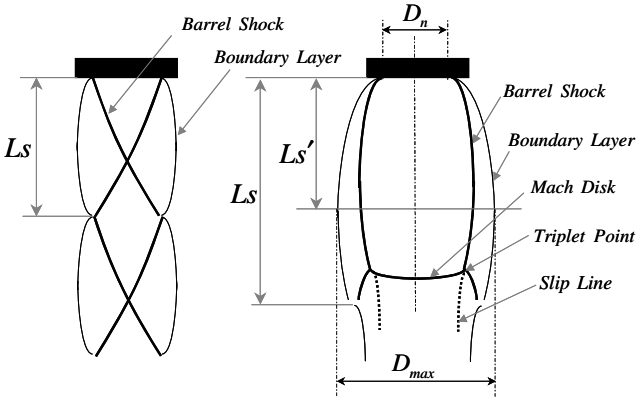

a) Under the low pressure ratio b) Under the high pressure ratio

Fig. 18 Definition of the shock cell length.

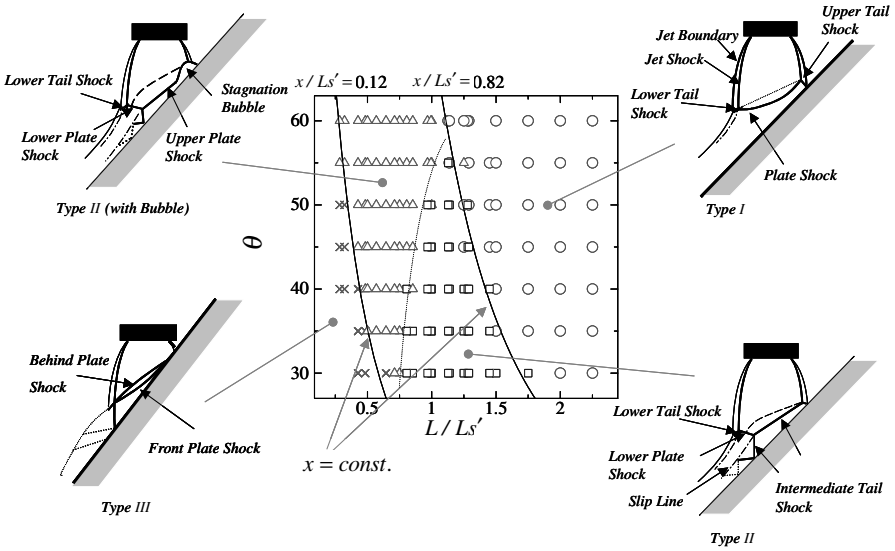

Fig. 19 Classification of the flow patterns.

cases, but $\theta = 30$ deg and $L/D_n = 2.0$ for Fig. 16a, and $\theta = 50$ deg and $L/D_n = 1.0$ for Fig. 16b. Similarly, Figs. 17a and 17b show the Schlieren images of the same Type II flowfield. The pressure ratio PR is 7.0 in both cases, but $\theta = 30$ deg and $L/D_n = 3.0$ for Fig. 17a, and $\theta = 45$ deg and $L/D_n = 2.0$ for Fig. 17b. The flowfield under certain conditions shows the same flow pattern as that under the condition of a smaller plate angle and a larger distance.

Horizontal lines are intentionally drawn in both Figs. 16 and 17. They show the location of the jet boundary hitting on the flat plate. x, vertical distances from the jet exit to the location of the jet hitting the plate, are almost the same for Figs. 16a and 16b. The same is true for Figs. 17a and 17b. As has already been shown in Figs. 14a–14c, the flowfields seem to be divided and classified into three types by the curves of x/D_n being constant. x/D_n is an important factor that determines the flow pattern.

When observing the plots in Figs. 14a–14c globally, we may notice that the whole plots seem to shift from left to right as pressure ratio increases. Pressure ratio is directly related to the shock cell length of the freejet; therefore the influence of pressure ratio may be removed when L/D_n is replaced with L/L_s and the three plots in Figs. 14a–14c may be unified. Generally, when the pressure ratio is low, an underexpanded supersonic jet forms some continuous shock cell structures as schematically shown in Figs. 18a and 18b. However, for the high-pressure ratios considered in the present experiment, shock cell structures are not clearly formed. Therefore, instead of normalization by the shock cell length L_S, normalization by L'_S, the distance from the nozzle exit to the location at the maximum diameter of the barrel shock structure, is used. The replotted result using L/L'_S as a horizontal axis is shown in Fig. 19. Also plotted are the curves of constant x/L'_S. All the points are summarized and plotted in one figure. This figure shows that the flow pattern can be estimated without any experiment. It is true that the L'_S depends on pressure ratio, but L'_S (or shock cell length L_S) can easily be obtained theoretically, or by a simple computation or experiment of freejets without flat plates. Suppose we generate the chart of L'_S or L_S vs pressure ratio in advance; plots like Fig. 19 can tell which type of the flowfield would appear under the given geometrical conditions. That is, the flow pattern can be estimated without any experiment, as all the other parameters are purely geometrical. The estimation of the flow pattern is important as it is related to the pressure peaks on a flat plate.

There is another curve plotted in Fig. 19. As mentioned earlier, there are cases with a stagnation bubble and without a bubble in the Type II flowfield. The angle of the jet impingement over the plate seems to be the key parameter for the classification of bubble existence, but additional experiments are necessary to draw conclusions.

V. Conclusions

The flow structure formed by the jet impingement on the inclined flat plate at various angles was investigated with the experimental observation of the pressure maps obtained by the PSP and the images of Schlieren pictures. The temperature dependency of PSP was removed by temperature calibration using the TSP technique and flowfield discussion became possible based on the measurements using the PSP technique and Schlieren images.

From the experiment performed at various flat plate angles, the flow patterns were classified by the observation of the shock wave configurations and the pressure maps. It became clear that the Type II has the stagnation bubbles at high-pressure ratios. All the three types of flowfield can be observed even for other flow and geometrical conditions.

The flowfields were classified in terms of nozzle-plate distance and plate angle. The distance from the nozzle lip to the point where the jet shock first impinges on the plate was found to be a key parameter in changing the flow pattern. By replacing the effect of pressure ratio into the shock cell distance, or into the distance from the nozzle lip to the location of the maximum barrel width, all the three plots under different pressure ratios were unified into one plot. This result indicates that flow type can be estimated when the flat plate angle and nozzle-plate distance are given and the shock cell length is known in advance.

The result obtained also indicated that extensive studies for a wide range of geometrical and physical parameters became feasible with a new efficient PSP/TSP measurement technique that shows surface pressure map with much less effort compared to conventional pressure tap measurement.

Acknowledgments

This research is partially supported by the "Molecular Sensors for the Aero-Thermodynamic research (MOSAIC)" program, the special coordination founds of the Ministry of Education, Culture, Sports, Science and Technology. The authors would like to thank Keisuke Asai, the leader of this program, and other members for stimulating discussions on the PSP and TSP techniques used in the present study.

References

[1] Carling, J. C., and Hunt, B. L., "The Near Wall Jets of Impinging, Uniform, Axisymmetric, Supersonic Jet," *Journal of Fluid Mechanics*, Vol. 66, Pt. 1, 1974, pp. 159–176.

[2] Kalghatgi, G. T., and Hunt, B. L., "The Occurrence of Stagnation Bubbles in Supersonic Jet Impingement Flows," *Aeronautical Quarterly*, Vol. 27, Aug. 1976, pp. 169–185.

[3] Lamont, P. J., and Hunt, B. L., "The Impingement of Underexpanded, Axisymmetric Jets on Perpendicular and Inclined Flat Plates," *Journal of Fluid Mechanics*, Vol. 100, Pt. 3, 1980, pp. 471–511.

[4] Al-Qutub, A. M., and Budair, M. O., "Experiments on the Flow over a Flat Surface Impinged by a Supersonic Jet," AIAA Paper 95-2935, 1995.

[5] Kim, K.-H., and Chang, K. S., "Three-Dimensional Structure of a Supersonic Jet Impinging on an Inclined Plate," *Journal of Spacecraft and Rockets*, Vol. 31, No. 5, 1994, pp. 778–782.

[6] Wu, J., Tang, L., Luke, E. A., Tong, X.-L., and Cinnella, P., "Comprehensive Numerical Study of Jet-Flow Impingement over Flat Plates," *Journal of Spacecraft and Rockets*, Vol. 39, No. 3, 2002, pp. 357–366.

[7] Bell, J., Schairer, E. T., Hand, L. A., and Mehta, R. D, "Surface Pressure Measurements Using Luminescence Coatings," *Annual Review of Fluid Mechanics*, Vol. 33, 2001, pp. 155–206.

[8] Liu, T. S., Guille, M., and Sullivan, J. P., "Accuracy of Pressure Sensitive Paint," AIAA Paper 99-3785, 1999.

[9] Fujii, K., Tsuboi, N., and Fujimatsu, N., "Visualization of Jet Flows over a Plate by Pressure—Sensitive Paint Experiments and Comparison with CFD," *Visualization and Imaging in Transport Phenomena*, Vol. 972, New York Academy of Sciences, New York, 2002, pp. 265–270.

[10] Rabek, J. F., *Mechanics of Photophysical Processes and Photochemical Reactions in Polymers: Theory and Applications*, John Wiley & Sons, New York, 1987.

[11] Fujimatsu, N., Tamura, Y., and Fujii, K., "Improvement of Noise Filtering and Image Registration Methods for the Pressure Sensitive Paint Experiments, " *Journal of Visualization*, Vol. 8, No. 3, 2005, pp. 225–233.

[12] Tsuboi, N., Hayashi, K., Fujiwara, T., Arashi, K., and Kodama, Y., "Numerical Simulation of a Supersonic Jet Impingement on a Ground," SAE 1991 Transactions, *SAE Transactions, Section 1, Journal of Aerospace*, Vol. 99, Pt. 2, 1991, pp. 2168–2180.

H. Chelliah
Associate Editor